Available online at www.sciencedirect.com
ScienceDirect
Optics Communications 272 (2007) 197–204
OPTICS COMMUNICATIONS
www.elsevier.com/locate/optcom

Manufacture of pupil filters for 3D beam shaping

C. Ibáñez-López, L. Muñoz-Escrivá, G. Saavedra, M. Martínez-Corral *

Departamento de Óptica, Universidad de Valencia, 46100 Burjassot, Spain

Received 23 June 2006; received in revised form 31 October 2006; accepted 2 November 2006

Abstract

In a previous work we presented a new method for binarizing pupil filters designed to control the three-dimensional (3D) irradiance distribution in the focal volume of apodized systems. The method is based in the fact that the 3D amplitude point spread function of an axially-symmetrical system can be recovered entirely from a one-dimensional (1D) set of regularly spaced amplitude samples. Hence we proposed the use of 1D iterative Fourier transform algorithm to binarize a, properly mapped, version of the amplitude transmittance of the filter. The binary masks obtained consist of a set of opaque and transparent concentric annular zones. In this paper we have built two of these masks with opposing properties and we have experimentally verified their abilities in a focusing system. These experimental results strongly agree previous theoretical predictions.

1. Introduction

The control of beam structure in the three-dimensional (3D) region surrounding the focal point of focusing systems is an important task in various applications such as conventional imaging systems [1–3], optical data storage readout heads [4–6], optical tomography [7,8] where although the axial resolution is determined by spectral bandwidth of the light source, the transverse resolution and the focal depth are determined by the focusing system, or in confocal scanning microscopy [9]. Specifically, in confocal and multiphoton scanning microscopes the amplitude distribution in the image of a point source, that is, the 3D amplitude point spread function (PSF) of the system, is a matter of interest. Therefore, several efforts have been addressed to control its shape by the use of radially-symmetric pupil filters [10–16].

The manufacture of pupil filters in which the amplitude transmittance is a continuous function of the radial coordinate is a difficult task. In the case of purely absorbing filters a possible method to overcome this difficulty is to replace them by binary functions obtained by means of digital halftoning [17]. The resulting binary elements can be easily produced by light plotters of laser printers.

Iterative halftoning algorithms [18–25] constitute an important class of a wide scope of digital halftoning methods [26]. They can be used for both binarization of images and computation of binary diffractive optical elements. Taking into account the computational effort we consider the iterative Fourier transform algorithm (IFTA) one of the most effective iterative halftoning procedures. It is especially well suited for the computer generation of match filters and Fourier transform holograms [27], nevertheless it can be used for binarization of images as well [28,29].

In our previous papers we developed several digital halftoning techniques, among others one derived from classical IFTA, to binarize radially-symmetric continuous-tone pupil filters [30,31]. The resulting annular binary filters preserved the symmetry of their gray-level counterparts. The algorithm was initially used to generate pupil filters for shaping the axial profile of the 3D PSF [31]. But in [32] we demonstrated that in the case of radially-symmetric pupils it is possible to shape the whole 3D behavior of the PSF by means of annular binary filters which are computed by 1D IFTA. This is of great importance from the

* Corresponding author. Tel.: +34 963544718; fax: +34 963544715.
E-mail addresses: cristina.ibanez@uv.es (C. Ibáñez-López), genaro.saavedra@uv.es (G. Saavedra), manuel.martinez@uv.es (M. Martínez-Corral).

0030-4018/$ - see front matter © 2006 Elsevier B.V. All rights reserved.
doi:10.1016/j.optcom.2006.11.005

point of view of 3D imaging, as in confocal or multiphoton microscopy, for instance. In that paper we showed theoretically how to shape the 3D light-field distribution about the focus by using an iterative procedure in which both object and spectral constraints are imposed on one-column matrices. To this end we computed binary versions of axially-superresolving and Gaussian pupil filters by using the above mentioned algorithm. The resulting calculated 3D PSFs closely approximated those of their gray-tone counterparts. The interpretation of the obtained results is given in terms of the axial sampling expansion for 3D PSF [33,34].

Now, in this paper we experimentally demonstrate that the use of these binary filters in a focusing system operate as promised. We have constructed both binary filters and measured the 3D response of an apodized focusing system. Experimental results clearly agree the previous theoretical predictions. Note that, although realized in a paraxial configuration, the results of our experiment can be extrapolated to a non-paraxial context in the case of the axial response. The exact extrapolation of the transverse response does not hold.

2. The axial form of the sampling theorem

Let us start by considering the normalized amplitude PSF of an aberration-free telecentric system (see Fig. 1) that is apodized by a purely absorbing radially-symmetric pupil filter [35,36], namely

$$h(u,v) = 2\pi \int_0^1 t(\rho)\exp(-\mathrm{i}2\pi u\rho^2)J_0(v\rho)\rho\,\mathrm{d}\rho. \tag{1}$$

In Eq. (1) the function $t(\rho)$ represents the, properly scaled, amplitude transmittance of the pupil filter being ρ the radial coordinate in the pupil plane. The axial and transverse positions in the focal volume have been specified through the nondimensional generalized longitudinal and transverse coordinates

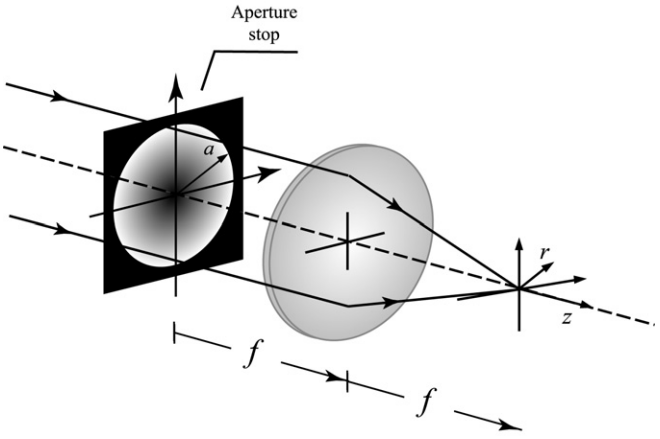

Fig. 1. Whatever focusing system we deal with, it can be schematized by means of an aperture stop, under plane wave illumination, and a converging spherical lens.

$$u = \frac{a^2}{2\lambda f^2}z \tag{2}$$

and

$$v = \frac{2\pi a}{\lambda f}r \tag{3}$$

respectively [37]. As shown in Fig. 1, z and r are the actual axial and transverse coordinates, respectively, and f is the focal length of the system.

In order to obtain the diffracted amplitude at any point in the focal volume, once the axial distribution of the latter is known, it is convenient to express the pupil function as a product of the circle function and a function, t_{P}, periodic in ρ^2 whose unit-cell transmittance is, precisely, that of the pupil function. In mathematical terms

$$t(\rho) = t_{\mathrm{P}}(\rho)\cdot \mathrm{circ}(\rho). \tag{4}$$

Since $t_{\mathrm{P}}(\rho)$ is periodic in ρ^2, it can be expressed in terms of a Fourier series as

$$t_{\mathrm{P}}(\rho) = \sum_{m=-\infty}^{+\infty} C_m \exp(\mathrm{i}2\pi m\rho^2), \tag{5}$$

where, of course, coefficients

$$C_m = \int_0^1 t(\rho)\exp(-\mathrm{i}2\pi m\rho^2)\rho\,\mathrm{d}\rho. \tag{6}$$

By comparing Eq. (6) with Eq. (1) one obviously has that

$$C_m = h(m,0)/2\pi. \tag{7}$$

Then, the 3D normalized amplitude PSF of the system can be expressed, by substituting Eqs. (4), (5) and (7) into Eq. (1), as

$$h(u,v) = \sum_{m=-\infty}^{+\infty} h(m,0)\int_0^1 \mathrm{circ}(\rho)\exp[-\mathrm{i}2\pi(u-m)\rho^2]J_0(v\rho)\rho\,\mathrm{d}\rho. \tag{8}$$

In other words

$$h(u,v) = \frac{1}{2\pi}\sum_{m=-\infty}^{+\infty} h(m,0)h_{\mathrm{C}}(u-m,v), \tag{9}$$

where $h_{\mathrm{C}}(u,v)$ represents the normalized 3D amplitude PSF corresponding to the case of the circular aperture.

This relevant formula, which constitutes the axial form of the sampling theorem [32], indicates that the 3D amplitude PSF of an apodized system results from the coherent superposition of an infinite number of properly axially shifted PSFs corresponding to the circular aperture. The shifts are equal to integer numbers. The weighting-factors set of this superposition is built, precisely, by sampling the axial PSF of the pupil filter in the axial nulls of the circular-aperture PSF. In other words, the 3D PSF of an apodized system may be fully determined from a set of sampling points that are regularly space along the optical axis, and the 3D PSF of the clear circular aperture. It is

usual in practice to express the latter in terms of Lommel functions [37].

As a trivial example of the above statement we may consider the case of the circular aperture. In this case the sampled values are zero at all sampling points save the one corresponding to $m = 0$. Therefore the trivial result $h(u, v) = h_C(u, v)$ is obtained.

Since function $h(u, v)$ is completely determined by the value of $h(u, 0)$ at $u = 0, \pm 1, \pm 2, \ldots$ (we assume that the circular-aperture PSF is known), it is convenient to express function $h(u, 0)$ in a simpler form. To that we perform the following geometrical nonlinear mapping

$$\mu = \rho^2 - 0.5; \quad q(\mu) = t(\rho). \tag{10}$$

Then, the axial amplitude PSF can be written, aside for an irrelevant phase factor, in the following way

$$h(u, 0) = \pi \int_{-0.5}^{0.5} q(\mu) \exp(-i2\pi u\mu)\, d\mu. \tag{11}$$

Since $q(\mu)$ and $h(u, 0)$ constitute Fourier transform pair, $h(u, 0)$, which is a band-limited function, can be completely recovered, according to sampling theorem, from a set of its properly spaced samples.

3. 1D iterative Fourier transform algorithm

As established in Section 2, the 3D amplitude PSF of an apodized system is fully determined by a discrete set of values of the 1D Fourier transform of the mapped transmittance $q(\mu)$. It is then clear that, if we are interested in obtaining a binary mask which reproduces the focal-volume structure corresponding to pupil filters designed to control the 3D amplitude PSF, it is precisely $q(\mu)$ the function which should be binarized. To reach this aim an algorithm specially designed for obtaining strong resemblance between the low-frequency spectra, at the proper sampled points, of the function $q(\mu)$ and its binary counterpart, $q_B(\mu)$, should be used. Then, the 1D version of the IFTA appears as an adequate binarization technique. Moreover, since during the execution of the algorithm only the values of the spectrum of $q(\mu)$ at a discrete number of equidistant points are of interest, the use of fast Fourier transform procedure to perform the different Fourier transformations, does not constitute a numerical short cut, but the natural and most efficient solution to this calculation problem.

The flow chart of the IFTA is presented in Fig. 2. The operators used in the algorithm are defined as follows:

$$U^{(k)} q_j(\mu) = \begin{cases} 0, & |q_j(\mu)| \leqslant e^{(k)}, \\ 1, & |q_j(\mu)| > 1 - e^{(k)}, \\ |q_j(\mu)|, & \text{otherwise}, \end{cases} \tag{12}$$

and

$$H\tilde{q}_j(u) = \begin{cases} \beta_j |\tilde{q}(u)| \exp\{i\theta(u)\}, & u \in S, \\ \tilde{q}_j(u), & \text{otherwise}, \end{cases} \tag{13}$$

where $\theta(u) = \arg\{\tilde{q}_j(u)\}$.

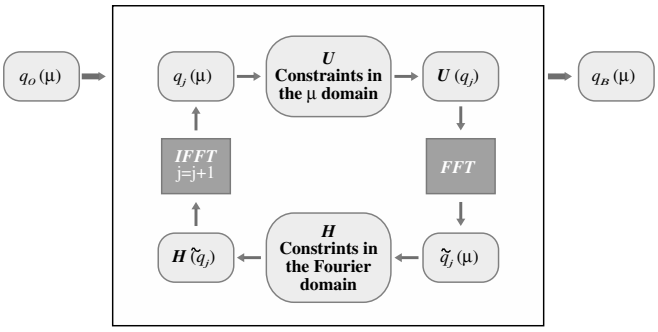

Fig. 2. The flow chart of IFTA.

The algorithm starts with the function $q(\mu)$ sampled in M equidistant points. Then, the discrete function undergoes a nonlinear transformation by the operator U. The modified function, $U(q_j(\mu))$, is Fourier transformed (by FFT algorithm) and then the function $\tilde{q}_j(u)$ is obtained. Now Fourier domain constraints H are imposed. After this modification the function is inversely Fourier transformed to the spatial domain and U is again applied on it.

The operator U is a tunable nonlinear function which allows one to avoid the stagnation of the algorithm [27]. The parameter $e^{(k)} \in [0, 0.5]$ is increased after a number of iterations. Finally U approaches the thresholding operator. Thus the final loops of the iterations are executed with the hardclip ($e^{(k)} = 0.5$). The operator H represents the constraints in the Fourier domain. In the predetermined region S it substitutes the modulus of the spectrum of the modified function by the modulus of the spectrum of the original continuous-tone function. The proportionality coefficient

$$\beta_j = \frac{\sum_{u \in S} |\tilde{q}_j(u)|^2}{\sum_{u \in S} |h(u, 0)||\tilde{q}_j(u)|}, \tag{14}$$

which minimizes the quadratic deviation of $|\tilde{q}_j(u)|$ from $|h(u, 0)|$ over the window S, is calculated in each iteration. When the procedure terminates, the inverse mapping of $q_B(\mu)$ into the ρ domain leads to the actual filter consisting of a set of M concentric annular zones of equal area.

4. The binary filters

The viability of the proposed method has been established in two experiments. On the one hand we consider the axially-superresolving parabolic filter, whose amplitude transmittance is $t(\rho) = (2\rho^2 - 1)^2$, or after the mapping $q(\mu) = 4\mu^2$ (see Eq. (10)). This filter provides a significant narrowness of the central lobe of the axial PSF, but accompanied by a severe enlargement of outer sidelobes. Moreover, the central lobe of the transverse PSF remains almost unaffected. On the other hand, we consider the Gaussian filter $t(\rho) = \exp(-\pi^2\rho^2)$, or $q(\mu) = \exp(-\pi^2(0.5 + \mu))$. The filters have been chosen with the intention of checking the accuracy of our method in two quite different situations. In one case we deal with a filter that compresses the focal volume. On the contrary, the Gaussian filter provides an expansion of it.

We aimed to get binary filters supporting 3D amplitude PSFs that closely approximate those of the gray-tone counterparts in a given volume surrounding the focal point. In most of cases of interest the diffracted field surrounding the focal point is vanishing small, except for a small volume that encloses this point. Therefore, according to the axial sampling theorem, we set the axial interval, A, where $\tilde{q}_{\mathrm{B}}(u)$ should be virtually identical with $h(u,0)$, symmetrical about the focal point and bounded by the third axial null (positive and negative) of the circular-aperture PSF.

To start the algorithm the function $q(\mu)$ was sampled, for both filters, in $M = 33$ equally spaced points. At this point a remark should be made about practical implementation on the algorithm. It is known that when the FFT algorithm is applied to calculate the spectrum of a function of compact support sampled at, for example, M points, it is usual to surround it by zeros and form a vector of $N > M$ pixels. This is done to obtain a sufficiently dense sampling in the spectrum. Note that our aim here is to obtain strong resemblance between the spectrum of the binary mask, $\tilde{q}_{\mathrm{B}}(u)$, and the one of its continuous-tone counterpart, $h(u,0)$, in the axial points of coordinates $u = 0$, ± 1, ± 2, and ± 3. Then it is mandatory that such points coincide with the sampling points in the Fourier domain. It is easy to find that to fulfill this constraint the ratio N/M must be integer. Now the question is to find out which is the optimum value for the ratio. In this context it should be considered that if the algorithm is performed by setting $N = M$, the binarization noise, inherent to the use of digital-halftoning techniques, is transferred to the high-frequency part of the spectrum. On the contrary, if $N/M > 1$ the binarization noise is transferred not only to outer parts but also to points within the low-frequency area such that $u \neq m$ (note that also in this case the substitution region S only includes integer values for u). In our experiments, as a result of a comprehensive trial-an-error study, we established that no improvement in terms of SNR is achieved by setting $N > M$. In other words, an increase in the size of the one-column matrices used in the algorithm does not improve the results and only increase the computational effort. Therefore, we formed a vector composed by $M = 33$ pixels.

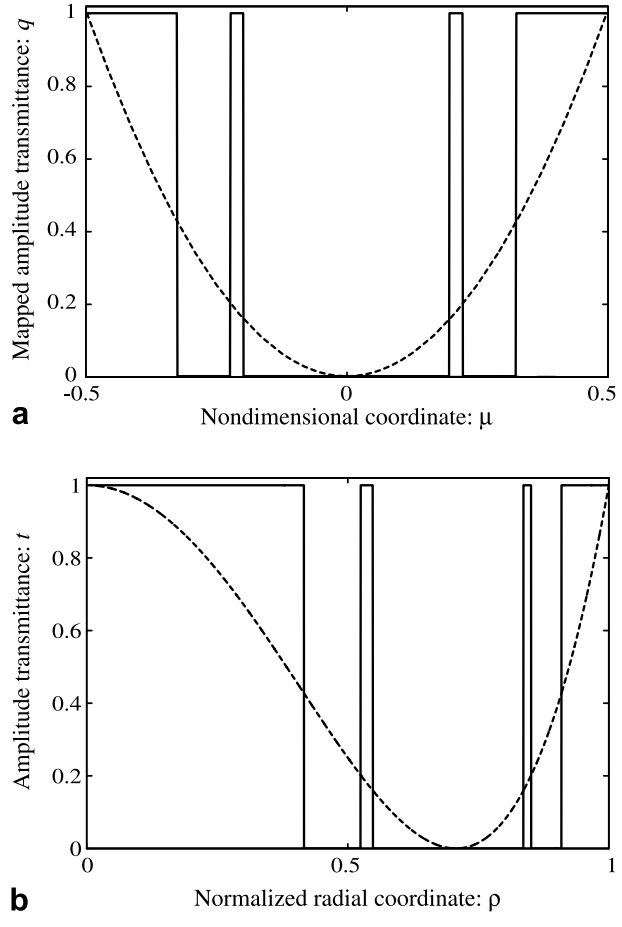

Fig. 3. Binary version of the axially-superresolving filter obtained by 1D IFTA for $M = 33$: (a) representation in the μ space and (b) representation in the ρ domain. The broken curves represent the amplitude transmittance of the continuous-tone filter.

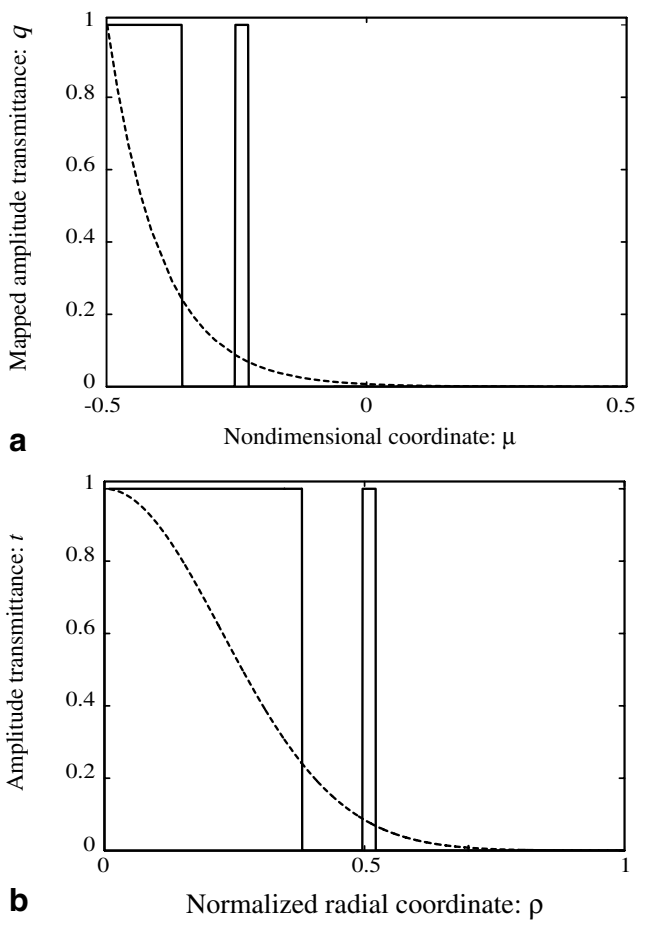

Fig. 4. Binary version of the Gaussian filter obtained by 1D IFTA for $M = 33$: (a) representation in the μ space and (b) representation in the ρ domain. The broken curves represent the amplitude transmittance of the continuous-tone filter.

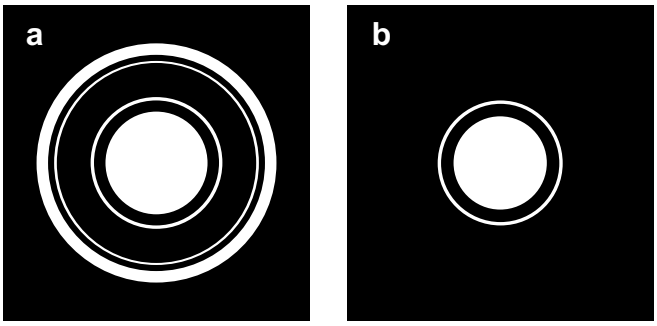

Fig. 5. Actual 2D representation of the binary filters: (a) parabolic filter and (b) Gaussian filter.

The $1 \times M$ column matrix served as the input for the IFTA algorithm. To continue with the algorithm three free parameters should be fixed. The parameters are: the interval by which $e^{(k)}$ is increased, the number of iterations between the changes from $e^{(k)}$ to $e^{(k+1)}$, and the extension of the spectral region S in which spectrum values are substituted. During the experiment we found that the size of spectral-exchange regions influences the SNR. Specifically we found that when S is centered about the focal point and includes the four first axial nulls of the circular-aperture PSF, the SNR is maximized. That is, we found optimal S to be slightly wider than A.

As regards the parameter $e^{(k)}$ we found in our experiment that its optimum value is filter dependent. Specifically we deduced, after a trial-and-error procedure, that for the case of the axially-superresolving parabolic pupil filter, the parameter $e^{(k)}$ must be increased from 0.025 to 0.5 by 0.025. On the contrary, for the case of the Gaussian filter it was found that $e^{(k)}$ should be increased from 0.01 to 0.5 by 0.01. In both cases we found that the number of iterations between $e^{(k)}$ and $e^{(k+1)}$ should be equal to two. A further increase in the number of iterations did not influence the result and only increased the time of computation.

The amplitude transmittances of the binary filters obtained by the 1D iterative technique are shown in Figs. 3 and 4. In both figures the dashed curves represent the transmittances for the continuous counterparts, in the μ and the ρ domains respectively. In Fig. 5 we show the filters in their actual two-dimensional form. Note that both binary filters correspond to continuous filters with the same radial extent.

5. Experimental results

To show the behavior of the designed filters we have measured the 3D response of a focusing system when the binary filters act as the entrance pupil of the system. The scheme of the experimental setup it is shown in Fig. 6. The monochromatic light proceeding from a CW, He–Ne laser ($\lambda = 632.8$ nm) propagates through a monomode optical fiber of NA = 0.08. Both elements constitute a Gaussian source of 5 μm in diameter placed at the front focal plane of the collimating lens L_1 ($f = 125$ mm and $\phi = 50.8$ mm). Since the beam emerging from the lens is still basically Gaussian, we can assume that its waist, ω, is at the back focal plane of L_1 and about $\omega = 10$ mm. As we see below, the binary filter has an outer most radius of 1.5 mm. Thus, we could assume in good approximation that the beam emerging from the lens illuminated uniformly the binary filter, which was located at the front focal plane of the focusing lens L_2 ($f = 381$ mm). This configuration conferred the system the property of telecentricity and consequently the intensity distribution in the neighborhood of the back focal plane of L_2 is symmetric respect to such plane.

The detector used is a CCD camera (AP1E from Apogee) mounted on a micrometric translation stage over an optical rail which permits the displacement along the optical axis (which we will hereafter call z-axis). Thus the beam profile generated in the focal region of the focusing system can be captured at different axial distances. Later processing of this set of 2D images provides the whole 3D intensity PSF of the system. The CCD chip (type KAF-4100E from Kodak) consists of a grid of 768×512 pixels (9 μm × 9 μm) equipped with a 14-bit analog-to-digital converter which allows to obtain information even from regions of the focal volume with very low intensity.

Before the acquisition of the images, the CCD camera was calibrated to compensate possible pixel errors and to determine the conditions under it works in the linear regime. After the acquisition of the diffraction patterns, each frame registered was corrected from bias and dark current.

The binary filters were built by photolithographic methods with an outer diameter of 3 mm. Since we worked with an optical rail with 50 cm travel, there was a twofold limit on the aperture sizes that we could use. If the radius of the

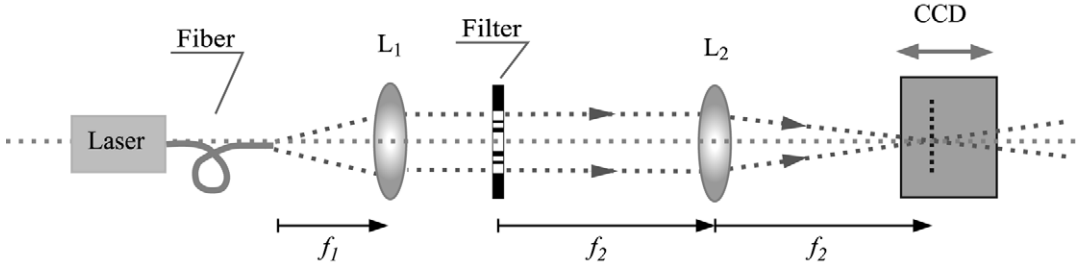

Fig. 6. Experimental setup for the characterization of the binary filters in a focusing system.

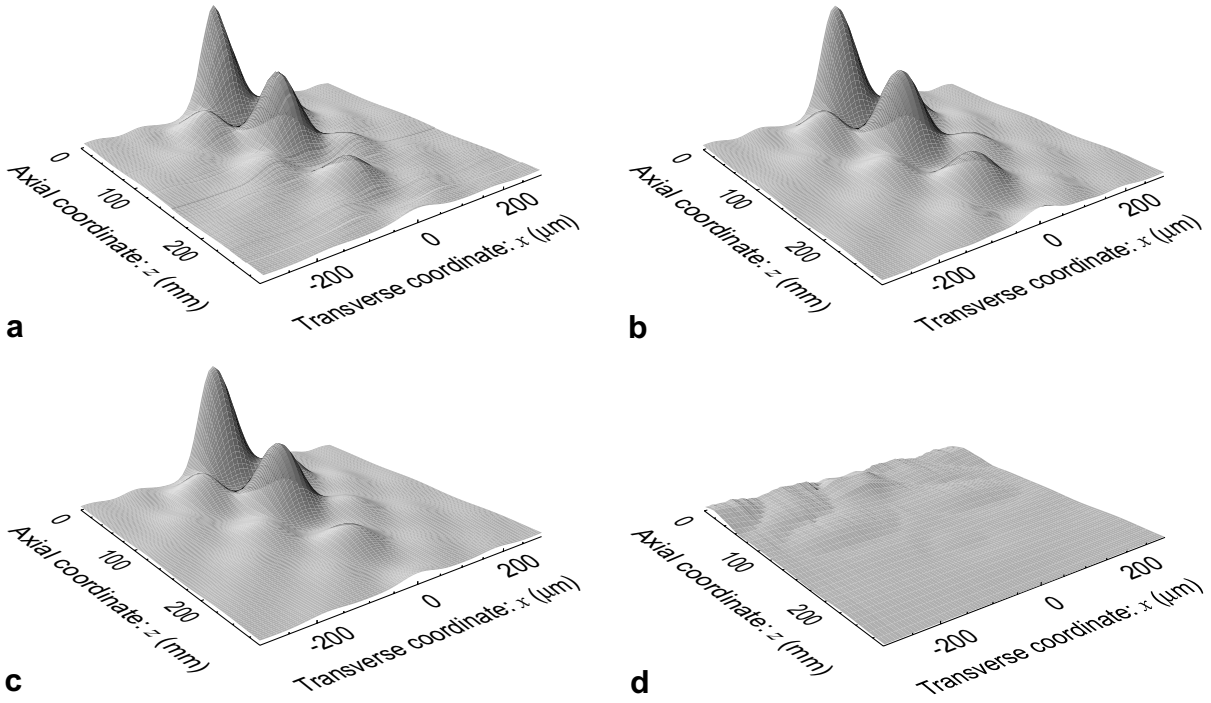

Fig. 7. (a) Experimental 3D PSF of the focusing system apodized with the binary superresolving filter; (b) numerically evaluated 3D PSF for the same binary filter; (c) numerically evaluated 3D PSF of the continuous version of the filter; and (d) map of absolute values of difference between the experimental and the calculated PSFs of the binary filter.

aperture is too large, then the focal spot is too little and the CCD cannot resolve it. If, in contrast, the radius is small, then the axial extent of the 3D pattern is too long and, therefore, due to the limited length of the optical rail, the image of the third axial null of the superresolving profile cannot be acquired. Because of that we selected an outer

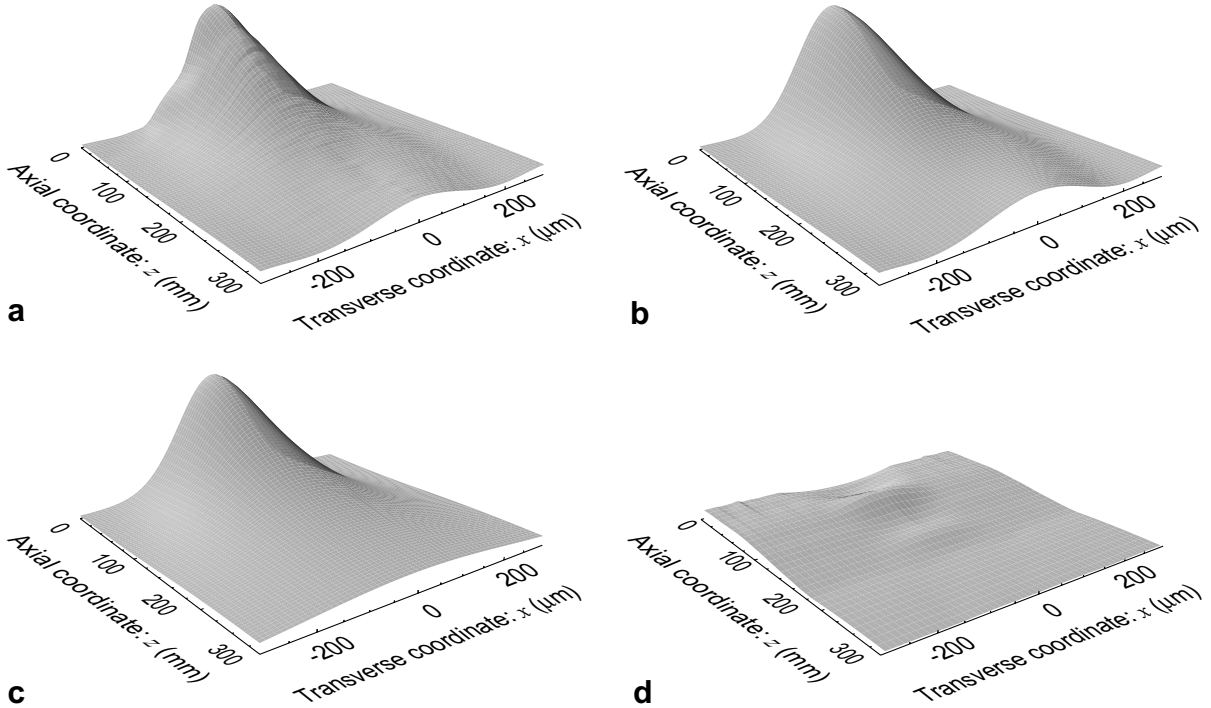

Fig. 8. (a) Experimental 3D PSF of the focusing system apodized with the binary Gaussian filter; (b) numerically evaluated 3D PSF for the same binary filter; (c) numerically evaluated 3D PSF of the continuous version of the filter; and (d) map of absolute values of difference between the experimental and the calculated PSFs of the binary filter.

radius of 1.5 mm. With this radius, the diameter of the central lobe of the focal spot is about 14 pixels of the CCD, which provide very high resolution images, and the third axial null is still within the optical rail.

After an axial scanning of the CCD we obtained a set of 2D images corresponding to the transversal patters in the focal volume of the system at different z positions. The proper combination of these images gives the whole 3D intensity distribution. The experimental 3D PSF measured for the focusing system apodized with the superresolving filter is shown in Fig. 7a. We also show the numerically-evaluated 3D PSF corresponding to the binary filter, Fig. 7b, and to the continuous version of the filter, Fig. 7c. It is apparent that the PSF of the binary filter closely approximates to that of the continuous one. To illustrate the accuracy of our measurements we have calculated the differences between the experimental and calculated PSFs of the binary filter, which are plotted in Fig. 7d.

In Fig. 8 we present the results corresponding to the Gaussian filter. As in the previous case, experimental measurements confirm the results predicted by the theory. In this last experience we have demonstrated the possibility to reproduce the 3D intensity distribution of a Gaussian beam with a very simple pupil filter, which just consists of two transparent centred rings.

The strong resemblance between theoretical and experimental results confirm the numerical calculations presented in [32] and demonstrate, on the one hand, that 1D IFTA algorithm provides binary filters whose 3D response closely approximates the intensity distribution generated by the corresponding filters of continuous amplitude transmittance. On the other hand, the experimental results prove the fact that the use of amplitude filters constitutes one of the more efficient techniques devoted to shape the 3D response of a focusing system. Its low-cost and the slight modifications required in the system architecture contribute to the success of this technique.

6. Conclusions

We have demonstrated, experimentally, the possibility to control the 3D structure of the focal volume in focusing systems by means of the binarized version of radially-symmetric purely-absorbing pupil filters specifically designed to this end. The binarization method, which we thoroughly explained in a previous paper [32], is based on the use of a properly adapted version of IFTA which is applied to a mapped transmittance of the filter. Although we deal with 3D fields we only need to apply the Fourier tools to one-column matrices. As follows from the axial sampling theorem, the 3D PSF of an apodized system can be recovered with a set of regularly spaced axial samples. Hence, our algorithm uses matrices with a very low number of pixels. Therefore our approach exhibits a highly remarkable time-computing efficiency when compared with other usual 2D algorithms. This efficiency could be very useful to implement, in real time, radially-symmetric pupil filters by means of programmable liquid-crystal spatial light modulators [38].

To confirm the viability of our method we carried out two experimental measurements. One with a filter that compresses the focal field, the other with a filter that expands it. In both cases, the resulting annular binary mask provided a experimental 3D irradiance PSF that closely approximates the one provided by the corresponding gray-tone counterpart. This strong agreement of the experimental results with the theoretical predictions reveals, not only the capabilities of the 1D IFTA to provide binary filters which exhibit a very similar behavior to that of the continuous counterpart but the efficiency of the use of amplitude transmittance filters to control the 3D PSF of a focusing system.

Acknowledgement

This work was supported by the Plan Nacional I+D+I (Grant DPI2003-4698), Ministerio de Ciencia y Tecnología, Spain.

References

[1] P. Jacquinot, B. Rozien-Dossier, Apodisation, in: E. Wolf (Ed.), Progress in Optics, vol. III, North-Holland, Amsterdam, 1964.
[2] P.S. Carney, G. Gbur, J. Opt. Soc. Am. A 16 (1999) 1638.
[3] T.R.M. Sales, Phys. Rev. Lett. 81 (1998) 3844.
[4] G. Bouwhuis, J. Braat, A. Huijser, J. Pasman, G. Van Rosmalen, K. Schouhamer, Principles of Optical Disc Systems, Adam Hilger, Bristol, 1985.
[5] R. Kant, J. Mod. Opt. 47 (2000) 905.
[6] M. Martínez-Corral, P. Andrés, C.J. Zapata-Rodríguez, M. Kowalczyk, Opt. Commun. 165 (1999) 267.
[7] D. Huang, E.A. Swanson, C.P. Lin, J.S. Schuman, W.G. Stinson, W. Chang, M.R. Hee, T. Flotte, K. Gregory, C.A. Pulifiato, J.G. Fujimoto, Science 254 (1991) 1178.
[8] L. Thrane, H.T. Yura, P.E. Andersen, J Opt. Soc. Am. A 173 (2000) 484.
[9] J.B. Pawley (Ed.), Handbook of Biological Confocal Microscopy, Plenum Press, New York, 1995.
[10] C.J.R. Sheppard, Optik 99 (1995) 32.
[11] M. Martínez-Corral, P. Andrés, C.J. Zapata-Rodríguez, C.J.R. Sheppard, Optik 107 (1998) 145.
[12] M. Martínez-Corral, M. Kowalczyk, C.J. Zapata-Rodríguez, P. Andrés, Appl. Opt. 37 (1998) 6914.
[13] S. Grill, E.H.K. Stelzer, J. Opt. Soc. Am. A 16 (1999) 2658.
[14] C.J.R. Sheppard, Opt. Lett. 24 (1999) 505.
[15] M.A.A. Neil, R. Juskaitis, T. Wilson, Z.J. Laczik, Opt. Lett. 25 (2000) 245.
[16] M. Kowalczyk, C. Zapata, E. Silvestre, M. Martínez-Corral, Opt. Appl. 28 (1998) 127.
[17] M. Kowalczyk, T. Cichocki, M. Martínez-Corral, V. Kober, Pur. Appl. Opt. 4 (1995) 553.
[18] S.A. Seldowitz, J.P. Allebach, D.W. Sweeney, Appl. Opt. 26 (1987) 2788.
[19] M. Broja, F. Wyrowski, O. Bringdahl, Opt. Commun. 69 (1989) 205.
[20] J. Turunen, A. Vasara, J. Westerhold, Opt. Eng. 28 (1989) 1162.
[21] W. Xiaolin, Visual Comput. 11 (1994) 69.
[22] T. Zeggel, O. Bringdahl, Opt. Commun. 118 (1995) 5.
[23] T. Scheermesser, O. Bringdahl, J. Elect. Im. 4 (1995) 179.
[24] T. Zeggel, O. Bringdahl, Proc. SPIE 2567 (1996) 456.
[25] J.P. Allebach, Proc. SPIE 3299 (1998) 26.
[26] R. Ulichney, Digital Halftoning, MIT Press, Cambrigde, 1987.

[27] T. Peter, F. Wyrowski, O. Brigdahl, J. Mod. Opt. 40 (1993) 591.
[28] R. Mrusek, M. Broja, O. Bringdahl, Opt. Commun. 75 (1990) 5.
[29] M. Kowalczyk, P. Sokolowski, EOS Top. Meet. Digest Ser. 12 (1997) 182.
[30] M. Kowalczyk, M. Martínez-Corral, T. Cichocki, P. Andrés, Opt. Commun. 114 (1995) 211.
[31] T. Cichocki, M. Martínez-Corral, M. Kowalczyk, P. Andrés, J. Mod. Opt. 45 (1998) 227.
[32] M. Martínez-Corral, L. Muñoz-Escrivá, M. Kowalczyk, T. Cichocki, Opt. Lett. 26 (2001) 1861.
[33] H. Arsenault, A. Boivin, J. Appl. Phys. 38 (1967) 3988.
[34] J.E.A. Landgrave, L.R. Berriel-Valdos, J. Opt. Soc. Am. A 14 (1997) 2962.
[35] C.J.R. Sheppard, P. Török, J. Opt. Soc. Am. A 15 (1998) 3016.
[36] M. Martínez-Corral, L. Muñoz-Escrivá, A. Pons, Appl. Opt. 40 (2001) 3164.
[37] M. Born, E. Wolf, Principles of Optics, Pergamon, Oxford, 1987 (Chapter 8).
[38] J.A. Davis, J.C. Escalera, J. Campos, A. Marquez, M.J. Yzuel, C. Iemmi, Opt. Lett. 24 (1999) 628.